Int. J. Electrochem. Sci., 14 (**2019**) 5188 – 5199, doi: 10.20964/2019.06.10

International Journal of
ELECTROCHEMICAL
SCIENCE
www.electrochemsci.org

Preparation of Porous Silicon by Electrochemical Etching Methods and its Morphological and Optical Properties

Junwen Xu[1], *Shuang Liu*[1,*], *Yapei Yang*[1], *Jiacheng Li*[1], *Chunhui Tian*[1], *Lina Guo*[1], *Shangjian Zhang*[1], *Yong Liu*[1], *Zhiyong Zhong*[1]

[1] University of Electronic Science and Technology of China, State Key Laboratory of Electronic Thin Films and Integrated Devices, School of Optoelectronic Science and Engineering, Chengdu 610054, China
[2] University of Electronic Science and Technology of China, School of Electronic Science and Engineering, Chengdu 610054, China
[*]E-mail: shuangliu@uestc.edu.cn

Received: 14 January 2019 / *Accepted:* 12 March 2019 / *Published:* 10 May 2019

Porous silicon (PS) has been widely used in solar cells and photodetectors because of its very low reflectance. However, its properties are greatly influenced by its morphological characteristics. In this work, PS samples with different morphologies were prepared by electrochemical etching with different fabrication parameters (etching time, current density, and solution composition). There were cracks microstructures on the surface of PS and their shapes were affected by different fabrication parameters. A crack model was established to analyze the formation mechanism of the surface morphology. The influence of different fabrication parameters on the surface morphology and the infrared spectrum of PS were analyzed. The morphological and optical properties of PS with a composite structure were studied. The results indicated that PS with composite structure can promote the oxidation reaction while significantly reducing the reflectance.

Keywords: Porous silicon; Morphology; Optical properties; composite structure

1. INTRODUCTION

Silicon is widely used in today's semiconductor field because of its low price and high process compatibility. However, the application of silicon in the infrared is limited by its higher reflectance and its wide band gap [1, 2]. The emergence of porous silicon has effectively improved these limitations. Porous silicon has a sponge-like structure capable of reducing the reflectance [3] and exhibits the characteristics of a direct band gap semiconductor [4, 5]. Therefore, it has been widely used in solar

cells, photodetectors, and other wide-spectrum applications using visible to infrared light [6-8]. The most common fabrication method of porous silicon is electrochemical etching [9-11]. The morphology of porous silicon is affected by the fabrication parameters and its surface microstructures do not only consist of pores, but also ridges and cracks [7, 12]. Porous silicon is unstable when the etching conditions change, which ultimately leads to the degradation of the functional structures and cracking [13]. The mechanical instability of crack formation [14] determines the kinetics [15] and the luminescence [16-18]. However, the formation mechanism of the cracks and the relationship between the fabrication parameters and the various morphology are not yet well understood.

In this work, porous silicon was prepared by an electrochemical etching method and samples with various morphologies were obtained by changing the fabrication parameters. The surface morphology and the infrared (IR) spectra of the porous silicon were measured and a crack model was established to explain the crack formation mechanism for different fabrication parameters. The effects of different experimental fabrication parameters on the morphology were discussed in detail by combining the results with the information from the spectrum.

2. EXPERIMENTAL

Porous silicon samples were fabricated by electrochemical etching on a single-sided polished *p*-type silicon wafer with a resistivity of 8-20 Ω/cm. Before etching, the silicon substrates were cleaned by ultrasonication in 5% hydrofluoric acid solution for 5 min to remove the surface oxides and impurities. At the same time, a pre-etching pit was formed for smooth etching. The electrochemical etching setup used a copper sheet as the anode and a platinum sheet as the cathode. The backside of the polished silicon wafer was placed on the copper sheet so that only the front of the silicon wafer was in contact with the solution.

The main parameters influencing the experiment were the etching solution, the current density (J), and the etching time. The etching solution was prepared by mixing 40% hydrofluoric acid (HF), deionized (DI) water, and 99.8% ethanol in a given proportion, or by using 10% H_2O_2 instead of DI water. The concentration of hydrofluoric acid in the solution was varied from 6.67% to 10%. After the silicon wafer was cleaned, the porous silicon was etched by electrochemical anodic etching and the experiments were carried out at room temperature. During the etching of the porous silicon, a constant current source was used to control the current density. The current density varied from 13 to 40 mA/cm^2 and the etching time ranged from 25 to 110 min.

The samples obtained were analyzed by scanning electron microscopy (SEM) to characterize the surface topography. A Dektak-XT step meter was used to measure the cross-section profiles of the samples and analyze the local three-dimensional topography. The infrared (IR) measurements were carried out with a Tensor27 Fourier transform infrared (FTIR) spectrometer in the specular reflectance geometry and the spectra were obtained in the absorption mode. Since the porous silicon layer (psl) can be considered as a film, its reflectance can be measured using a Filmetrics F20 thin film analyzer.

3. RESULTS AND DISCUSSION

3.1. Effect of the etching time and crack formation mechanism

The experimental parameters for studying the effect of the etching time on porous silicon are shown in Table 1. Porous silicon samples were obtained using an electrolyte containing HF, DI water, and ethanol in the ratio 1:1:2 (solution S1) and the electrochemical etching process was performed at an anodic current density of 13 mA/cm^2 for 25-110 min. After anodization, the morphologies of the porous silicon samples were observed by SEM, as shown in Figure 1. The surface microstructure (about 1 μm) persisted for 25 minutes before cracks and ridges appeared. When the etching time increases, the size of the ridges increases from 10 μm to 100 μm as well as the size of the cracks. The tendency of such cracks increasing with etching time is consistent with other researchers' result [15, 16].

Table 1. Etching conditions for different etching time.

Solution	Current density (mA/cm^2)	Etching time (min)	Sample no.
$HF:H_2O:C_2H_5OH$=1:1:2 (**S1**)	13	25	#1
		60	#2
		90	#3
		110	#4

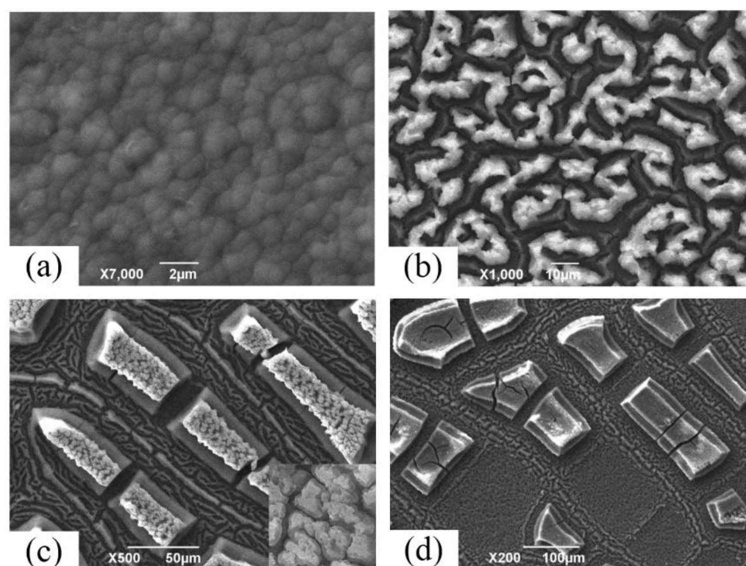

Figure 1. SEM images of the porous silicon samples at different etching times. (a) #1; (b) #2; (c) #3; (d) #4.

Cracks and ridges quickly appeared on the porous silicon and were attributed to the increase in surface force including the mechanical stress between the microstructure and the capillary forces in the pores [15]. Ethanol in the solution reduces the surface energy, thereby equaling the surface tension and the pressure to maintain structural stability. When the ethanol evaporates, the surface pressure becomes

greater than the surface tension, which leads to a loss in structural stability and extrusion deformation of the structure. The increase in surface pressure can be described by the Laplace equation [13]:

$$\Delta p = -\frac{2\gamma}{r} \tag{1}$$

In Eq. (1), Δp is the pressure differential, γ is the surface tension of the solution, and r is the radius of the pore. Eq. (1) indicates that the surface pressure per unit area of pore caused by the evaporation of the surfactant is unchanged if the solution remains the same. Figure 2(a) illustrates the model used and explains the mechanism of crack formation using the force and bending. By using the formula, the deflection and rotation of the porous silicon can be obtained as:

$$w_B = -\frac{ql^4}{8EI} \tag{2}$$

$$\theta_B = -\frac{ql^3}{6EI} \tag{3}$$

Where w_B is the disturbance to the bending, θ_B is the corner of the bend, q is the transverse pressure received, l is the height of the porous silicon, and EI is a constant. Porous silicon would offset the axis under the transverse pressure causing a large deformation and forming distinct ridge and crack structures. Figure 2(b) clearly indicates the inclined trace and the angle of the porous silicon. Therefore, this model can be used to qualitatively explain the structural characteristics of porous silicon.

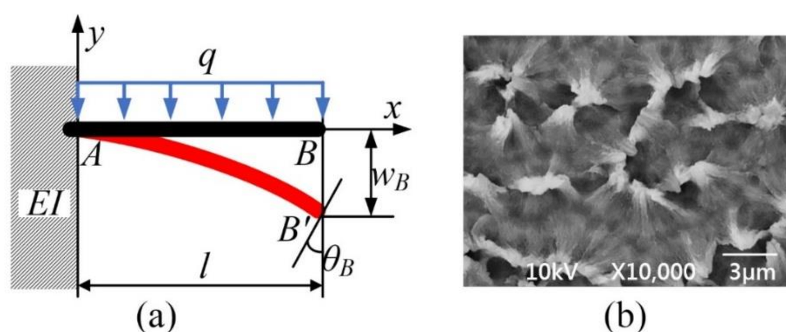

Figure 2. (a) Physical model for the crack formation mechanism; (b) SEM image of the PS after spraying with gold.

The three-dimensional images obtained with the step meter (Figure 3) show the height distribution in the porous silicon layer. The height of the porous silicon layer increased from 0.7 μm to 36 μm and the size of the ridges increased gradually with the same order when the etching time increases. The current density when the porous silicon dissolution mechanism evolves from longitudinal defect etching to electropolishing is called the critical current density. It is influenced by the experimental conditions [19]. When the current density is lower than the critical current density, electrochemical etching dominates over longitudinal defect etching. At a constant current, most of the carriers (holes) move to the interface between the silicon and the electrolyte, causing the silicon to gradually dissolve to create ridges and cracks on its surface.

The depth of the porous silicon layer (l) gradually increases with the etching time. According to Eq. (2) and (3), w_B and θ_B increase with l for the same transverse pressure. Therefore, the offset axis distance of the porous silicon increases, which makes the bending deformation larger than that of the sample with a smaller depth. A larger bending deformation makes the porous silicon aggregate into ridges, forming larger cracks and ridges. However, once the large depths induce a large deformation in

the porous silicon layer, the extrusion force between the porous silicon microstructure causes the ridge to split or even break away from the substrate. Figure 1(d) shows that the ridges are much larger than in the previous samples. Some ridges are separated from the substrate and only flat areas remain. At the same time, the pore size decreases as a result of extrusion deformation so that the surface of the island becomes gradually smoother.

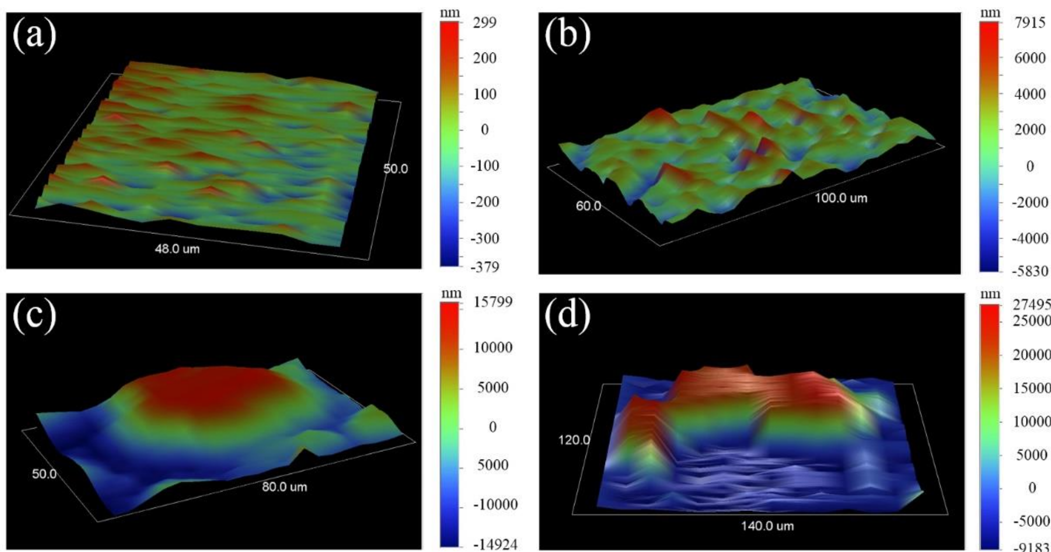

Figure 3. Three-dimensional images of the porous silicon at different etching time. (a) #1; (b) #2; (c) #3; (d) #4.

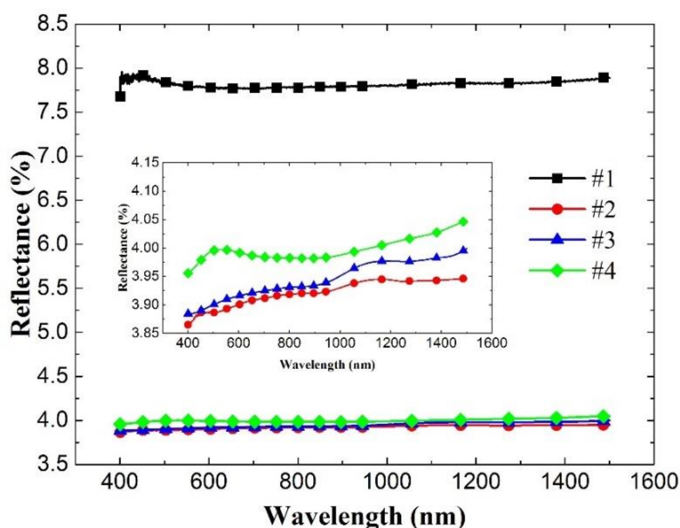

Figure 4. Reflectance of the porous silicon layer at different etching time.

The reflectance of the porous silicon samples was measured between 400 and 1500 nm, as shown in Figure 4. The reflectance first decreases then increases when the etching time increases and the minimum reflectance occurs after 60 min. This rule is consistent with previous studies, but the reflectance is lower than their minimum reflectance (about 6%) [20]. The depth of the porous silicon and the size of the ridges both affect the reflection of light. An appropriate depth and crack size could lead

to light trapping, which could increase the number of light reflections and effectively reduce the light reflectance. At the same time, small cracks on the surface of the ridges cause multiple reflections. For short anodization times, the small depth of the porous silicon layer results in a small number of effective reflections between the porous silicon microstructures, which ultimately leads to a higher reflectivity. For long anodization times, the large crack size and the microstructures detaching from the substrate reduce the number of reflections. The disappearance of the small cracks from the surface of the ridges causes direct reflection of the light, which increases the reflectance.

3.2. Effect of the etching current density

We then used the same solution S1 and set the etching time to 25 min while only changing the current density from 13 mA/cm^2 to 40 mA/cm^2. The experimental parameters are shown in Table 2. The surface morphology of the samples is shown in Figure 5. Slender ridges are formed and the cracks are much larger than the ridges, which is the same as the conclusion obtained by Mehrara [7]. When the current density increases, the number of holes participating in the reaction increase. The holes have enough energy to etch the walls so that lateral etching increases, which causes the ridges to become smaller and the cracks to become wider. The height of the porous silicon first increases slightly then decreases, indicating that the current density gradually exceeds the critical current density and electrochemical polishing occurs [21]. Excessive holes act on the walls until the space charge layer is etched away to make the silicon surface almost flat, as shown in Figure 6(b).

Table 2. Etching conditions for different current densities.

Solution	Current density (mA/cm^2)	Etching time (min)	Sample no.
$HF:H_2O:C_2H_5OH$=1:1:2 (**S1**)	13	25	#1
	20		#5
	25		#6
	40		#7

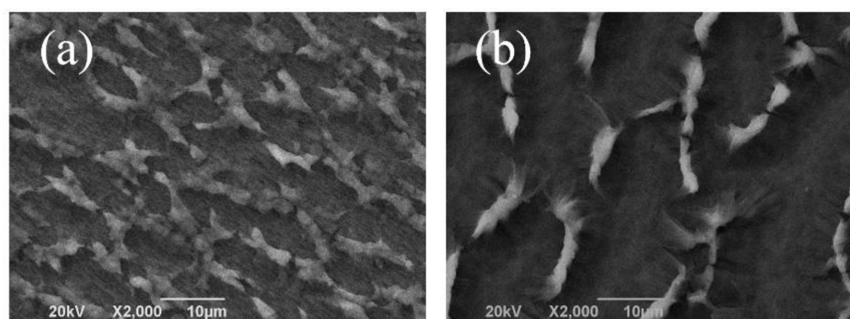

Figure 5. SEM images of the porous silicon for different current densities. (a) #5; (b) #6.

In Figure 7, the reflectance increases significantly when the current density increases. Porous silicon has distinct microstructures with different shapes and heights at low current densities, but the aspect ratio and the effective absorption thickness of the surface structure increase the number of

reflections in the porous silicon layer. As the current density exceeds the critical current density, the aspect ratio and the depth of the porous silicon layer decrease, which reduces the ability to capture light and the reflectance increases. The reflectance at 40 mA/cm^2 is close to the reflectance of planar pure silicon wafer, indicating that an electropolishing reaction has occurred.

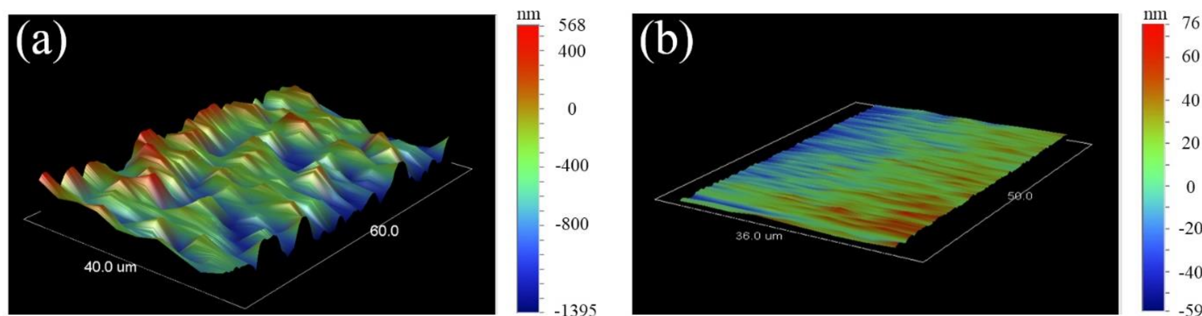

Figure 6. Three-dimensional images of the porous silicon for different current densities. (a) #5; (b) #7.

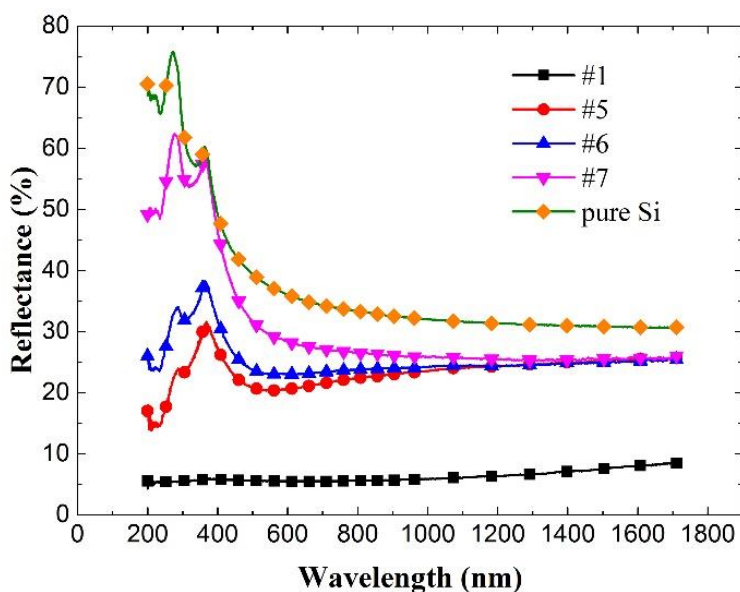

Figure 7. Reflectance of the porous silicon for different current densities.

3.3. Preparation and properties of PS with a composite structure

Table 3. Etching conditions with for different solution compositions.

Solution	Current density (mA/cm^2)	Etching time (min)	Sample no.
$HF:H_2O:C_2H_5OH$=1:2:3 (**S2**)	13	25	#8
	20		#9
$HF:H_2O_2:C_2H_5OH$=1:1:2 (**S3**)	13		#10
	20		#11

The island structure of the surface of sample #3 has cracks and a low reflectance. At the same time, the pore structure of porous silicon also has a good light trapping ability, so the preparation and

properties of composite structures with holes and cracks are discussed. The composite structure porous silicon was prepared by different methods and the preparation parameters are shown in Table 3.

Next, we kept etching time constant at 25 minutes while we varied the composition of the etching solution. One etching solution was HF, DI water, and ethanol in a ratio of 1:2:3 (solution S2), where the concentration of ethanol was still 50% but the concentration of hydrofluoric acid was changed from 10% to 6.67%. The topography of the porous silicon obtained at current densities of 13 and 20 mA/cm^2 is shown in Figure 8(a-b). When the concentration of hydrofluoric acid decreases, the amount of fluorine ions participating in the reaction decreases. When the current density is unchanged, the holes that are not consumed in time at the bottom of the pore start to move up towards the walls. Therefore, many cracks appear after 25 min of etching, as shown in Figure 8(a). The three-dimensional images of sample #8 (Figure 9(a)) illustrate the maximum etching height (about 500 nm) of the porous silicon layer. It is less than in sample #1 (700 nm, according to Figure 3(a)). The etching depth decreases as the HF concentration decreases, which is the same as the result presented by Zare [22]. When the current density increases to 20 mA/cm^2, many holes participate in the reaction and etch the wall to form sharp ridges. Figure 8(b) shows that a composite structure consisting of cracks and pores appears, but only a small number of holes are present between the cracks.

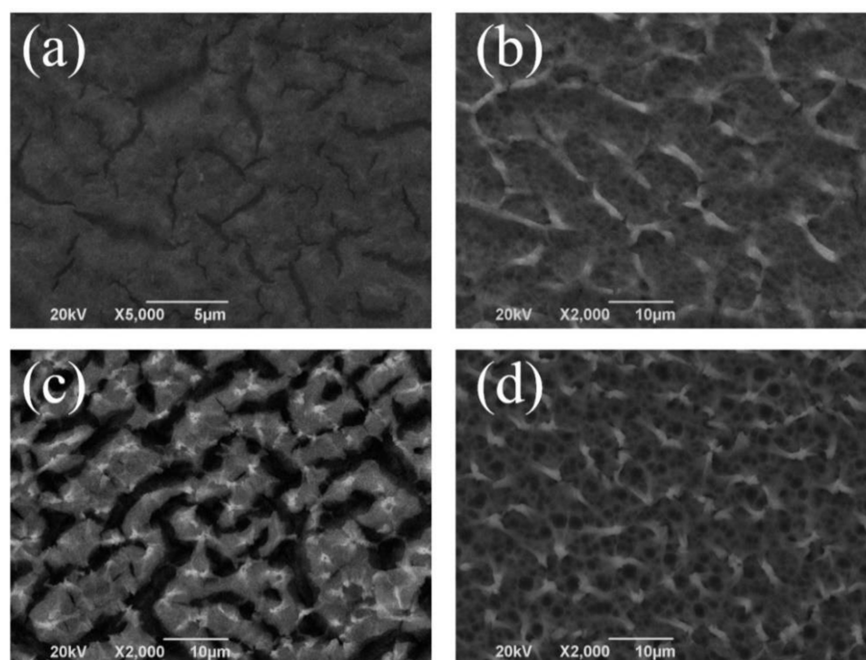

Figure 8. SEM images of the porous silicon for different etching solutions and current densities. (a) #8; (b) #9; (c) #10; (d) #11.

Another etching solution tested was HF, H_2O_2, and ethanol in the ratio of 1:1:2 (solution S3) where DI water was replaced with H_2O_2. The porous silicon samples obtained are shown in Figure 8(c-d). Figure 8(d) shows that a composite structure appeared as well, but the number of holes is larger and they all have a larger size. The three-dimensional image in Figure 9(b) indicates that the depth of the porous silicon layer etched with the H_2O_2 solution increases significantly, which is consistent with the

conclusions reported by Huang [23]. For the same etching current density and etching time, the strong H_2O_2 oxidant has a stronger ability to generate an anodic oxidation reaction. As a result, the silicon atoms are more easily oxidized to high valence states and both longitudinal and transverse etchings are favored, so that cracks occur earlier. Below the critical current density, the space charge layer protects the walls from being completely etched away, which prevents the occurrence of electrolytic polishing. As the experiment proceeds, pores are formed between the cracks, thereby forming a composite structure.

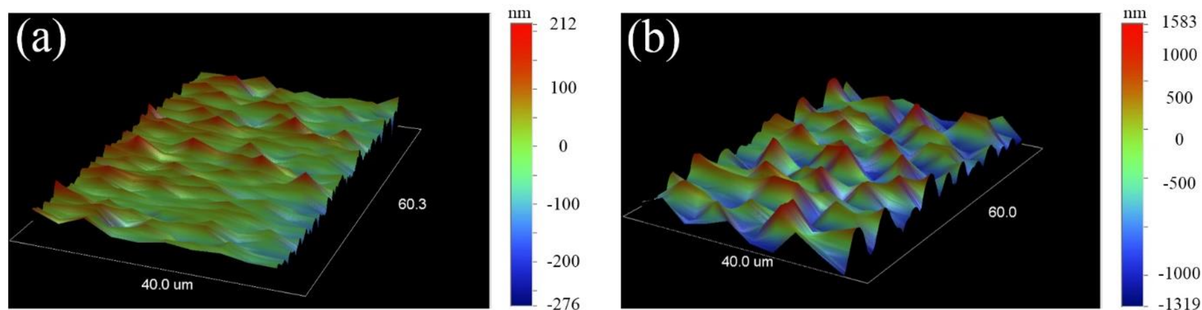

Figure 9. Three-dimensional images of the porous silicon. (a) #8; (b) #10.

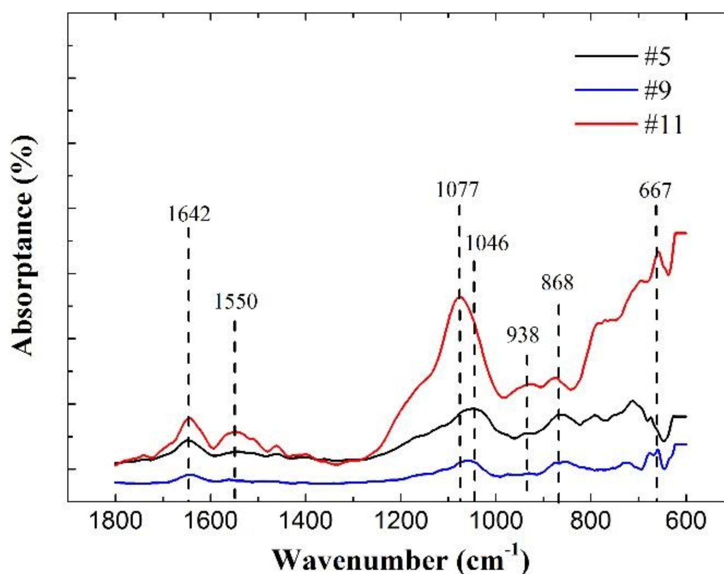

Figure 10. FTIR spectra of the porous silicon samples.

Table 4. FTIR vibrational frequencies for the main absorption bands in the 600-1800 cm^{-1} range.

Absorption band	Wavenumber [cm^{-1}]
Si-H_2	667
H_ySiO_x complexes	868, 938
SiF_4	1031
SiO_x	1046, 1077
H_ySiO_x complexes	1038, 1125
C-O	1642

Under different etching conditions, the formation of different composite structures can be analyzed by chemical bonds in the surface materials. Figure 10 shows the FTIR spectra of the porous silicon obtained with the three different solutions. As electrochemical etching proceeds, different chemical species are formed on the surface of the porous silicon. Table 4 shows the vibrational frequencies for the main absorption bands in the 600-1800 cm^{-1} range [24-28]. The peaks at 1642 and 1550 cm^{-1} correspond to carbon dioxide and nitrogen dioxide in the air, respectively, which is mainly due to an inaccurate background compensation during the measurements. Silicon will first be passivated and then oxidized in the hydrofluoric acid solution. Therefore, there will be a large amount of SiO_x and $Si\text{-}H_2$ bonds. The strong oxidation by H_2O_2 in solution S3 yields many Si-O bonds, which leads to the highest absorption peak. The silicon oxides are then etched by the fluoride ions and the main products are complexes of SiF_xH_y and H_ySiO_x. The absorption peak of solution S3 at 1077 cm^{-1} shifts to the left compared to solution S1 because the strong oxidation by H_2O_2 forms the silica oxide faster than it is etched by the fluoride ions, thereby resulting in a larger proportion of silicon oxide. Solution S2 also generates a slight left shift compared to solution S1, but for different reasons. The low concentration of fluoride ions in solution S2 makes the etching rate of the silicon oxide slower than its formation and the proportion of silicon oxide becomes larger.

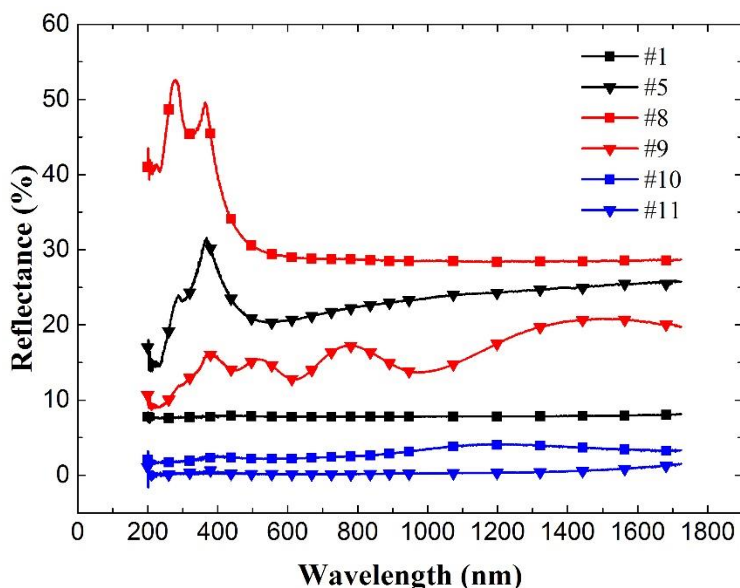

Figure 11. Reflectance of PS etched for 25 min using different etching solutions.

Figure 11 shows the reflectance of the porous silicon with composite structures. As the concentration of hydrofluoric acid changes to 6.67%, the etching rate of the longitudinal defects is much slower, which results in a decrease in the pore depth and an increase of the size of the cracks. Sample #8 has limited light trapping abilities because of the small microstructures and depth and the reflectance is higher than for sample #1. However, the reflectivity of sample #9 is lower than in sample #5 because the holes and cracks in the composite structure reflect the light more times. The reflectivity of sample #10 is less than that of sample #1 because the etching depth and the crack spacing of the porous silicon increase significantly under the strong oxidation action of H_2O_2. Sample #11 has the lowest reflectance,

which is attributed to the composite structure generated by H_2O_2. Light is first reflected between the ridges and then part of the light enters the holes and is reflected again. Some light is even repeatedly reflected in the composite structure. Therefore, a composite structure with more pores greatly reduces the reflectance in sample #11.

4. CONCLUSION

In this work, porous silicon was prepared by electrochemical anodic etching with different fabrication parameters (etching time, current density, and solution composition). Then, the effects of different etching conditions on the morphology and the IR spectrum were analyzed. A crack formation model was established to analyze the formation mechanism of the porous silicon surface morphology. The experimental results indicate that the longitudinal etching depth increases with the etching time and that cracks and ridges are gradually formed. Both structures affect light trapping in the porous silicon. When the etching current density increases, the reflectance increases and electrochemical polishing causes the surface topography to become smoother. Two methods were used to prepare the composite structures. The composite structure prepared using a low concentration of HF has less pores, but the reflectance is significantly reduced. The composite structure prepared using H_2O_2 has a more pores with a large size and has the lowest reflectance. Experiments showed that the composite structure can increase the light trapping ability of porous silicon and reduce its reflectivity, which can broaden the application range of porous silicon.

ACKNOWLEDGEMENTS
This work was supported by the National Natural Science foundation of China (Grant No.61734002, 61435010, 61177035 and 61421002). The authors would also like to thank CCD Research Center of China Electronics.

References

1. T.H. Her, R.J. Finlay, C. Wu, S. Deliwala, E. Mazur, *Appl. Phys. Lett.*, 73 (1998) 1673.
2. S.J. Ma, S. Liu, Q.W. Xu, J.W. Xu, R.G. Lu, Y. Liu, Z.Y. Zhong, *AIP Adv.*, 8 (2018), 035010.
3. O. Bisi, S. Ossicini, L. Pavesi, *Surf. Sci. Rep.*, 38 (2000) 1.
4. G.D. Sanders, Y.C. Chang, *Phys. Rev. B*, 45 (1992) 9202.
5. F. Buda, J. Kohanoff, M. Parrinello, *Phys. Rev. Lett.*, 69 (1992) 1272.
6. R. Bilyalov, L. Stalmans, G. Beaucarne, R. Loo, M. Caymax, J. Poortmans, J. Nijs, *Sol. Energy Mater. Sol. Cells.*, 65 (2001) 477.
7. H. Mehrara, A. Erfanian, M. Khaje, M. Zahedinejad, F. Raissi, F. Rezvani, *Sens. Actuators, A*, 184 (2012) 119.
8. G.M. Youssef, M.M. El-Nahass, S.Y. El-Zaiat, M.A. Farag, *Mater. Sci. Semicond. Process.*, 39 (2015) 457.
9. F. Raissi, M.S. Abrishamian, T. Emadi, *Ieee. Trans. Electron Devices*, 51 (2004) 339.
10. L.S. Chuah, Z. Hassan, H.A. Hassan, A.K. Yahya, S. Alam, *AIP Conf. Proc.*, 1250 (2010) 385.
11. A.G. Cullis, L.T. Canham, *Nature*, 353 (1991) 335.
12. S. Li, W. Ma, Y. Zhou, X. Chen, M. Ma, Y. Xiao, Y. Xu, *J. Lumin.*, 146 (2014) 76.
13. W. Qiu, Y.L. Kang, Q. Li, Z.K. Lei, Q.H. Qin, *Appl. Phys. Lett.*, 92 (2008) 041906.

14. G. Ulrike, Y. Arthur, *Thin Solid Films*, 255 (1995) 135.
15. D.S. Gaev, S.S. Rekhviashvili, *Semiconductors*, 46 (2012) 137.
16. D.M. Michael, J.S. Donald, K.B. Steven, *Thin Solid Films*, 406 (2002) 151.
17. B.M. Bulakh, N.E. Korsunska, L.Y. Khomenkova, T.R. Staraya, M.K. Sheĭnkman, *Semiconductors*, 40 (2006) 598.
18. M.E. Raypah, N.M. Ahmed, *Mater. Sci. Semicond. Process.*, 31 (2015) 235.
19. H. Föll, M. Christophersen, J. Carstensen, G. Hasse, *Mater. Sci. Eng. R*, 39 (2002) 93.
20. K. A. Salman, K. Omar, Z. Hassan, *Superlattices Microstruct.*, 50 (2011) 647.
21. A. Slimani, A. Iratni, J. N. Chazalviel, N. Gabouzec, F. Ozanamb, *Electrochim. Acta*, 54 (2009) 3139.
22. M. Zarea, A. Shokrollahia, F. E. Seraji, *Appl. Surf. Sci.*, 257 (2011) 9507.
23. Z. P. Huang, T. Shimizu, S. Senz, Z. Zhang, N. Geyer, Ulrich Gösele, *J. Phys. Chem. C*, 114 (2010) 10683.
24. Z.H. Wang, T. Urisu, H. Watanabe, K. Ooi, G. Ranga Rao, S. Nanbu, J. Maki, M. Aoyagi, *Surf. Sci.,* 575 (2005) 330.
25. A.P. Burtsev, V.N. Bocharov, S.K. Ignatov, T.D. Kolomiitsova, P.G. Sennikov, K.G. Tokhadze, L.A. Chuprov, D.N. Shchepkin, O. Schrems, *Opt. Spectrosc.*, 98 (2005) 227.
26. M.K. Weldon, K.T. Queeney, A.B. Gurevich, B.B. Stefanov, Y.J. Chabal, K. Raghavachari, *J. Chem. Phys.*, 113 (2000) 2440.
27. E. Díaz-Torres, G. Romero-Paredes, R. Peña-Sierra, A. Ávila-García, *Mater. Sci. Semicond. Process.*, 40 (2015) 533.
28. M. Kopani, M. Mikula, D. Kosnac, P. Vojtek, J. Gregus, E. Vavrinsky, M. Jergel, E. Pincik, *Appl. Surf. Sci.*, 461 (2018) 44.

© 2019 The Authors. Published by ESG (www.electrochemsci.org). This article is an open access article distributed under the terms and conditions of the Creative Commons Attribution license (http://creativecommons.org/licenses/by/4.0/).